Quasigeostrophic Vertical Motions Diagnosed from Along- and Cross-isentrope Components of the Q Vector

DANIEL KEYSER

Department of Atmospheric Science, State University of New York at Albany, Albany, New York

BRIAN D. SCHMIDT

WSI Corporation, Billerica, Massachusetts

DEAN G. DUFFY

Laboratory for Atmospheres, NASA/Goddard Space Flight Center, Greenbelt, Maryland

(Manuscript received 17 January 1991, in final form 12 July 1991)

ABSTRACT

In a recent paper on the kinematics of frontogenesis, Keyser et al. conjectured that partitioning the **Q** vector into along- and cross-isentrope components yields vertical-motion patterns that are respectively cellular and banded—the former on the scale of the baroclinic disturbance and the latter on the scale of the embedded frontal zones. This conjecture is examined diagnostically through solution of the quasigeostrophic omega equation, using the output from a nearly adiabatic and frictionless *f*-plane primitive equation channel model of the evolution of a baroclinic disturbance to finite amplitude. The results of the present study support the proposed conjecture, suggesting the following interpretation of the characteristic comma structure of the vertical-motion field in midlatitude baroclinic disturbances: The comma shape arises from the modification or distortion of a wave-scale dipole pattern by frontal-scale asymmetries. The dipole is associated with the along-isentrope component of the **Q** vector, reflecting the wavelike pattern in the potential temperature field within the baroclinic disturbance; the asymmetries are associated with the cross-isentrope component of the **Q** vector, reflecting the presence of frontal zones within the baroclinic disturbance.

1. Introduction

In a recent study of the kinematics of frontogenesis, Keyser et al. (1988; hereafter referred to as KRR) extended Petterssen's (1936; 1956, 200–202) classic frontogenesis equation, which relates the Lagrangian rate of change of the *magnitude* of the horizontal potential temperature gradient to invariant kinematic properties of the wind field, to include the rate of change of the *direction* of the horizontal potential temperature gradient. These quantities are the components of the Lagrangian rate of change of the horizontal potential temperature gradient $\nabla\theta$ in a natural Cartesian coordinate system (s, n) defined such that s is locally tangent to the isentropes and n is rotated 90° counterclockwise of s (KRR; Fig. 1). Referring to the Lagrangian rate of change d/dt of $\nabla\theta$ as **F**, KRR write

$$\mathbf{F} = F_s\mathbf{s} + F_n\mathbf{n}, \tag{1.1}$$

where

$$F_s = \mathbf{s}\cdot\frac{d}{dt}\nabla\theta, \tag{1.2a}$$

$$F_n = \mathbf{n}\cdot\frac{d}{dt}\nabla\theta. \tag{1.2b}$$

Noting that $\mathbf{n} = -|\nabla\theta|^{-1}\nabla\theta$ and $\mathbf{s} = \mathbf{n}\times\mathbf{k}$, KRR further show that

$$F_s = |\nabla\theta|\frac{d\alpha}{dt}, \tag{1.3a}$$

$$F_n = -\frac{d}{dt}|\nabla\theta|, \tag{1.3b}$$

where α is the orientation angle of the the isentropes (s axis) measured relative to the x axis (counterclockwise positive). Equations (1.3a) and (1.3b) respectively indicate that F_s is proportional to the rate of change of the direction of $\nabla\theta$ and F_n to the rate of change of the magnitude of $\nabla\theta$—the minus sign is necessary since **n** and $\nabla\theta$ are oppositely directed.

Corresponding author address: Prof. Daniel Keyser, Department of Atmospheric Science, ES-224, State University of New York at Albany, Albany, NY 12222.

A motivation for this generalization of Petterssen's frontogenesis equation is to reconcile the synoptic practices of 1) relating banded cloud and precipitation features in midlatitude baroclinic disturbances to patterns of F_n, and 2) inferring vertical motion from patterns of the quasigeostrophic (QG) forcing in terms of the divergence of the **Q** vector (Hoskins et al. 1978; Hoskins and Pedder 1980). The **Q** vector is defined as the contribution of the geostrophic flow to the rate of change of $\nabla_p\theta$ (the subscript p denoting partial differentiation on an isobaric surface) along a parcel trajectory. For adiabatic, horizontal QG flow, this definition reduces to the rate of change of $\nabla_p\theta$ along a trajectory defined by the geostrophic flow, that is,

$$\mathbf{Q} = \frac{d}{dt_g}\nabla_p\theta, \tag{1.4}$$

where $d/dt_g \equiv \partial/\partial t_p + \mathbf{V}_g \cdot \nabla_p$ (the subscript g denoting geostrophic). Keyser et al. (1988) propose reconciling the above synoptic practices by partitioning the divergence of the **Q** vector into natural-coordinate components $\nabla_p \cdot (Q_s\mathbf{s})$ and $\nabla_p \cdot (Q_n\mathbf{n})$, where Q_s and Q_n are the QG analogs of the components of **F** in (1.1)–(1.3). They pursue this objective using models that describe the evolution of a passive scalar field (i.e., potential temperature) in a specified horizontal wind field that is both nondivergent and steady state. Parameters are fixed such that QG scaling is valid (small Rossby number), allowing approximation of **F** by **Q**. Keyser et al. (1988) find that the patterns of vertical-motion forcing associated with $\nabla_p \cdot (Q_s\mathbf{s})$ and $\nabla_p \cdot (Q_n\mathbf{n})$ yield a scale separation in highly idealized flows isolating various kinematic properties of observed baroclinic disturbances. The forcing associated with $Q_s\mathbf{s}$ and $Q_n\mathbf{n}$ respectively produces cellular patterns on the scale of the baroclinic disturbance (wave scale) and banded patterns on the scale of the regions of enhanced baroclinicity (frontal scale) for idealized representations of a baroclinic wave and vortex. In the case of a linear band of isentropes embedded in a pure deformation field, the forcing associated with $Q_s\mathbf{s}$ is identically zero, so that the forcing is confined to $Q_n\mathbf{n}$, the component associated with frontogenesis in $|\nabla_p\theta|$. Thus, KRR conclude that use of Petterssen's definition of frontogenesis is qualitatively appropriate as long as it is understood to yield only a *frontal-scale* component of the vertical-motion field. The outcome of KRR also suggests the possibility of interpreting the well-known comma-shaped pattern of vertical motion in midlatitude baroclinic disturbances in terms of superpositions of the wave- and frontal-scale components deriving from the natural-coordinate partitioning of the **Q** vector.

The conclusions of KRR regarding a scale separation in the vertical-motion patterns in baroclinic disturbances are limited in several respects. First, their results are based on consideration of highly simplified flow models of a two-dimensional kinematic nature. Thus, the complication of vertical variations in the structure of baroclinic disturbances is not confronted. Second, by virtue of the two-dimensional kinematic formulation of these models, KRR only consider the implied *forcing* of vertical motion, where the vertical motion itself is the quantity of interest. The purpose of this paper is to address these limitations by partitioning the QG-diagnosed vertical motion into contributions associated with $Q_s\mathbf{s}$ and $Q_n\mathbf{n}$ in less restrictive flow configurations. For this purpose, we adopt the simulation of the evolution of a baroclinic wave disturbance to finite amplitude in a nearly adiabatic and frictionless f-plane primitive equation (PE) channel model described by Keyser et al. (1989; hereafter referred to as KSD). (The only nonconservative process explicitly included in the model is the fourth-order horizontal diffusion of potential temperature and the components of the horizontal wind velocity.) This simulation is considered sufficiently simple to remain comparable to the idealized flow models presented in KRR, yet sufficiently general for the conclusions potentially to have some bearing on baroclinic disturbances observed in nature. In addition to addressing the validity of the conclusions of KRR, the proposed natural-coordinate partitioning of the forcing of the QG omega equation will be used to interpret the structure of the comma-shaped pattern of vertical-motion characteristic of midlatitude cyclones observed in nature.

2. Decomposition of the vertical-motion field into along- and cross-isentrope components

The adiabatic, frictionless form of the QG omega equation in pressure coordinates (e.g., Hoskins and Pedder 1980) is

$$\sigma\nabla_p{}^2\omega + f_0{}^2\frac{\partial^2\omega}{\partial p^2} = -2h(\nabla_p \cdot \mathbf{Q}), \tag{2.1}$$

where

$$\mathbf{Q} = -\left(\frac{\partial \mathbf{V}_g}{\partial x}\cdot\nabla_p\theta\right)\mathbf{i} - \left(\frac{\partial \mathbf{V}_g}{\partial y}\cdot\nabla_p\theta\right)\mathbf{j} \tag{2.2}$$

is the **Q** vector (1.4) expressed in terms of horizontal gradients of geostrophic velocity and potential temperature. In (2.1) f_0 is a (constant) reference value of the Coriolis parameter and σ ($= -hd\Theta/dp$) is the static stability coefficient; ellipticity is guaranteed if this coefficient is positive. The quantity h [$=(\rho\theta)^{-1}$] is a function of pressure, which may be expressed equivalently as $h = (R/p_0)(p_0/p)^{c_v/c_p}$, where p_0 is a reference pressure (1000 hPa). The quantity Θ is a pressure-dependent reference profile of potential temperature, thus rendering σ a function of pressure alone. Unless noted to the contrary, the remaining notation is standard.

When solving (2.1), we separate the **Q** vector into

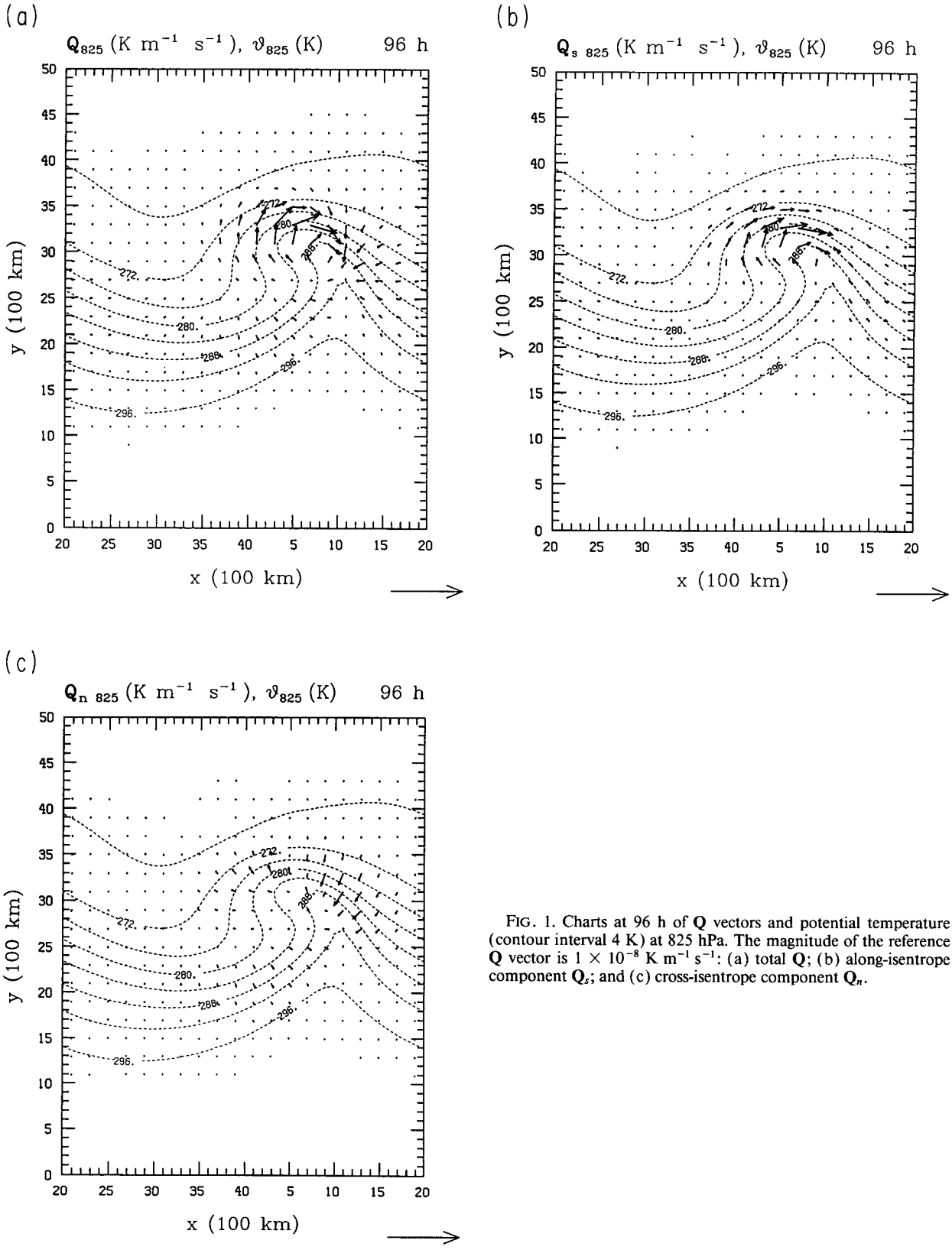

FIG. 1. Charts at 96 h of **Q** vectors and potential temperature (contour interval 4 K) at 825 hPa. The magnitude of the reference **Q** vector is 1×10^{-8} K m^{-1} s^{-1}: (a) total **Q**; (b) along-isentrope component $\mathbf{Q}_s$; and (c) cross-isentrope component $\mathbf{Q}_n$.

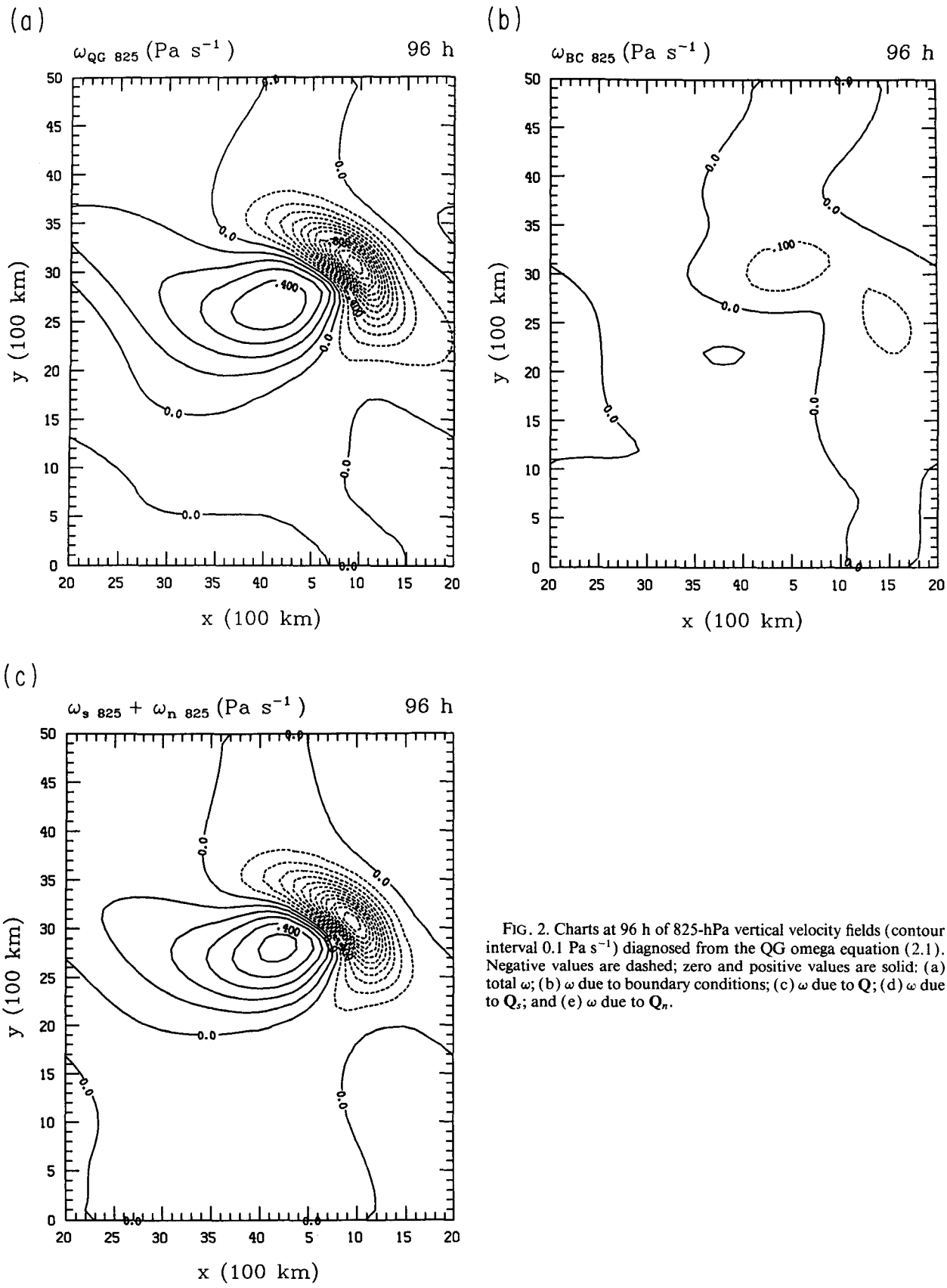

FIG. 2. Charts at 96 h of 825-hPa vertical velocity fields (contour interval 0.1 Pa s^{-1}) diagnosed from the QG omega equation (2.1). Negative values are dashed; zero and positive values are solid: (a) total ω; (b) ω due to boundary conditions; (c) ω due to $\mathbf{Q}$; (d) ω due to $\mathbf{Q}_s$; and (e) ω due to $\mathbf{Q}_n$.

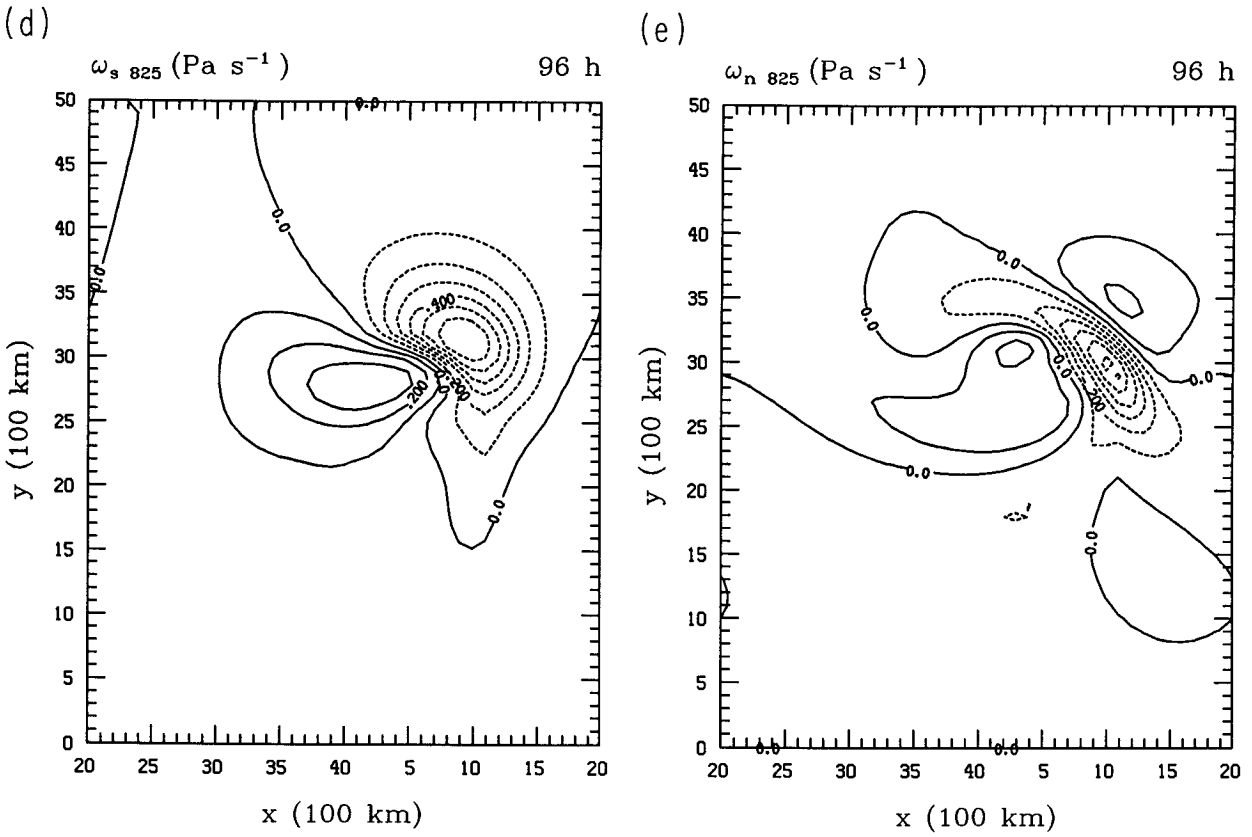

FIG. 2. (*Continued*)

natural-coordinate components analogous to (1.1)–(1.3). For notational convenience we write

$$\mathbf{Q} = \mathbf{Q}_s + \mathbf{Q}_n, \tag{2.3}$$

where $\mathbf{Q}_s \equiv Q_s\mathbf{s}$ and $\mathbf{Q}_n \equiv Q_n\mathbf{n}$. The Cartesian coordinate forms of Q_s and Q_n are not given here, but may be inferred from the forms of F_s and F_n presented in KRR [Eqs. (2.6b) and (2.6a)], with d/dt replaced by d/dt_g and the horizontal velocity replaced by its geostrophic counterpart. Equation (2.1) is solved numerically using successive overrelaxation on a subset of the PE model forecast domain (8000 km × 4000 km in the meridional and zonal directions), referred to in KSD (p. 2470) as the diagnostic domain and consisting of the inner 5000 km of the forecast domain in the meridional direction. The domain geometry is f-plane Cartesian; $f_0 = 1.03 \times 10^{-4}$ s^{-1}, which corresponds to 45°N. The horizontal grid is unstaggered with uniform spacing ($\Delta s = 100$ km); the vertical domain for solving (2.1) consists of 20 levels from 975 to 25 hPa, with uniform spacing ($\Delta p = 50$ hPa). The reference potential temperature profile $\Theta(p)$ is derived from horizontal averages of potential temperature on pressure surfaces on the model-forecast domain at the initial time of the simulation. The partitioned **Q** vector field (2.3) is evaluated from the model-simulated geostrophic velocity and potential temperature fields on the diagnostic domain. Boundary conditions for (2.1) are as follows: the vertical velocity ω is assumed periodic in the zonal direction, consistent with the channel geometry. The vertical velocity is set equal to the PE model values at the meridional and vertical boundaries; note that this results in $\omega = 0$ at the upper boundary (25 hPa). In the subsequent diagnoses based on (2.1), the QG ω field will be separated into contributions associated with the **Q** vector and its natural-coordinate components (2.3) for homogeneous meridional and vertical boundary conditions, and into a contribution associated with inhomogeneous lower and meridional boundary conditions and zero forcing.

3. Application to a channel-model simulation of baroclinic wave development

In this section, we examine the vertical velocity fields diagnosed from (2.1) at two times in the model integration that are considered in detail in KSD: 96 and 120 h of simulation time, where the surface cyclone and associated wave structure are amplifying and occluded, respectively (refer to Figs. 4 and 8 of KSD). At both times, the low-level (825 hPa) and midlevel (475 hPa) ω fields simulated in the PE model exhibit

the dipole structure characteristic of channel model simulations of cyclone structure and evolution (KSD; Figs. 6 and 10). Rather than consisting of circular cells of ascent and descent, the dipole pattern is composed of ellipses of ascent and descent, with the major axes respectively oriented along the low-level warm-frontal zone and the midlevel frontal zone. At the later time, the ellipses of ascent and descent are distorted significantly, especially at 825 hPa, with the combined patterns suggestive of the comma-cloud–dry-tongue structure commonly seen in visible satellite imagery of mature midlatitude cyclones. In view of the objective of interpreting the comma-shaped vertical-motion pattern, we investigate the relative contributions of $\mathbf{Q}_s$ and $\mathbf{Q}_n$ to the 825-hPa vertical velocity field using the QG omega equation, placing particular emphasis on explaining the structure of the asymmetries modifying the dipole pattern of ascent and descent.

a. Partitioned Q vectors and diagnosed vertical motion at 96 h

At 96 h, the 825-hPa $\mathbf{Q}$ pattern (Fig. 1a) is best defined at the crest of the thermal wave, where the $\mathbf{Q}$ vectors exhibit a substantial along-isentrope component (Fig. 1b).[1] The orientation of the $\mathbf{Q}_s$ vectors is in the sense of counterclockwise rotation of $\nabla_p\theta$, consistent with westward system-relative geostrophic flow through the crest of the thermal wave (not shown). The $\mathbf{Q}_s$ pattern results in the appearance of divergence on the southwestern flank of the thermal ridge and convergence on the northeastern flank, the latter region coinciding with the low-level warm-frontal zone. The cross-isentrope component of $\mathbf{Q}$ (Fig. 1c) displays vector patterns oriented toward the warm air along the warm- and cold-frontal zones, with the former the more prominent. The orientation of the $\mathbf{Q}_n$ vectors is consistent with Lagrangian increases in $|\nabla_p\theta|$ in the warm- and cold-frontal zones. The patterns of $\mathbf{Q}$, $\mathbf{Q}_s$, and $\mathbf{Q}_n$ in Fig. 1 bear some similarity to the corresponding patterns in Fig. 10 of KRR for a symmetric baroclinic vortex. The main discrepancy is that in the symmetric vortex the $\mathbf{Q}$ patterns are symmetric about the center, whereas in the channel simulation the patterns are better defined along the warm-frontal zone. The asymmetry in the channel simulation is a result of the stronger baroclinicity in the warm front relative to the cold front, whereas in the symmetric vortex both frontal zones are of equal strength, a consequence of the neglect of divergent flow in the vortex model.

The total QG ω field at 825 hPa (Fig. 2a) displays the characteristic dipole structure described previously, with the ascent concentrated into a relatively narrow band oriented along the warm-frontal zone, and the descent in the form of a broader band oriented along the midtropospheric frontal zone (KSD; Fig. 4d). The total QG ω pattern replicates the structure of its PE-simulated counterpart (KSD; Fig. 6a), but overestimates the amplitude. This discrepancy is a consequence of the overestimate of the strength of the flow by the geostrophic wind in cyclonic vortices, which is hypothesized to translate into too large a forcing in (2.1).[2] Further analysis of this discrepancy is provided by Keyser et al. (1992) in a detailed comparison of the QG-diagnosed and PE-simulated ω fields for the model under consideration here.

Figure 2b shows that the contribution of the boundary conditions to the ω field is minor. This contribution is due almost entirely to the lower boundary condition, the influence of which damps with altitude, since the total ω field (Fig. 2a) nearly vanishes along the meridional boundaries. Thus, the vertical velocity due to $\mathbf{Q}$ (Fig. 2c) can be used to interpret the structure of the total vertical velocity field. The ω patterns associated respectively with $\mathbf{Q}_s$ and $\mathbf{Q}_n$, to be referred to as ω_s and ω_n, are shown in Figs. 2d and 2e. The ω_s pattern exhibits a dipole composed of cellular patterns of descent and ascent, the centers of which correspond closely to the loci of divergence and convergence of $\mathbf{Q}_s$ noted earlier in the discussion of Fig. 1b. The ω_n pattern exhibits a narrow band of ascent coinciding with the warm-frontal baroclinicity along the northeastern side of the thermal ridge (Fig. 1c), the influence of which is directly apparent in the sum of ω_s and ω_n (Fig. 2c). There is a very weak hint of ascent on the warm side of the cold-frontal baroclinicity. Broad regions of relatively weak descent are found on each side of the thermal ridge, with the one on the southwestern side reinforcing the descent in the ω_s field found there (Fig. 2d). In this case, although there is not a clear scale separation between the ω_s and ω_n fields, there is a pattern separation, with the former yielding a cellular dipole pattern, and the latter contributing a well-defined banded feature with along- and cross-band scales comparable to the corresponding dimensions of the warm-frontal zone.

b. Partitioned Q vectors and diagnosed vertical motion at 120 h

We reexamine the partitioned $\mathbf{Q}$ vector and vertical-motion patterns at 120 h, a time at which the surface cyclone and baroclinic wave have reached the occluded stage of development. It is useful to examine the utility

[1] The reader is referred to the note by Sanders and Hoskins (1990) for a discussion relating distributions of $\mathbf{Q}$ vectors to various configurations of confluence, diffluence, and flow curvature typical of baroclinic disturbances.

[2] This argument is based on consideration of higher-order omega equations with less restrictive dynamical approximations (e.g., Eliassen 1984). The amplitude error in the dipole pattern also may be related to the neglect of dynamical properties of the flow in (2.1), such as locally varying static stability, baroclinicity, and inertial stability, which modulate the response of the vertical-motion field to a given forcing.

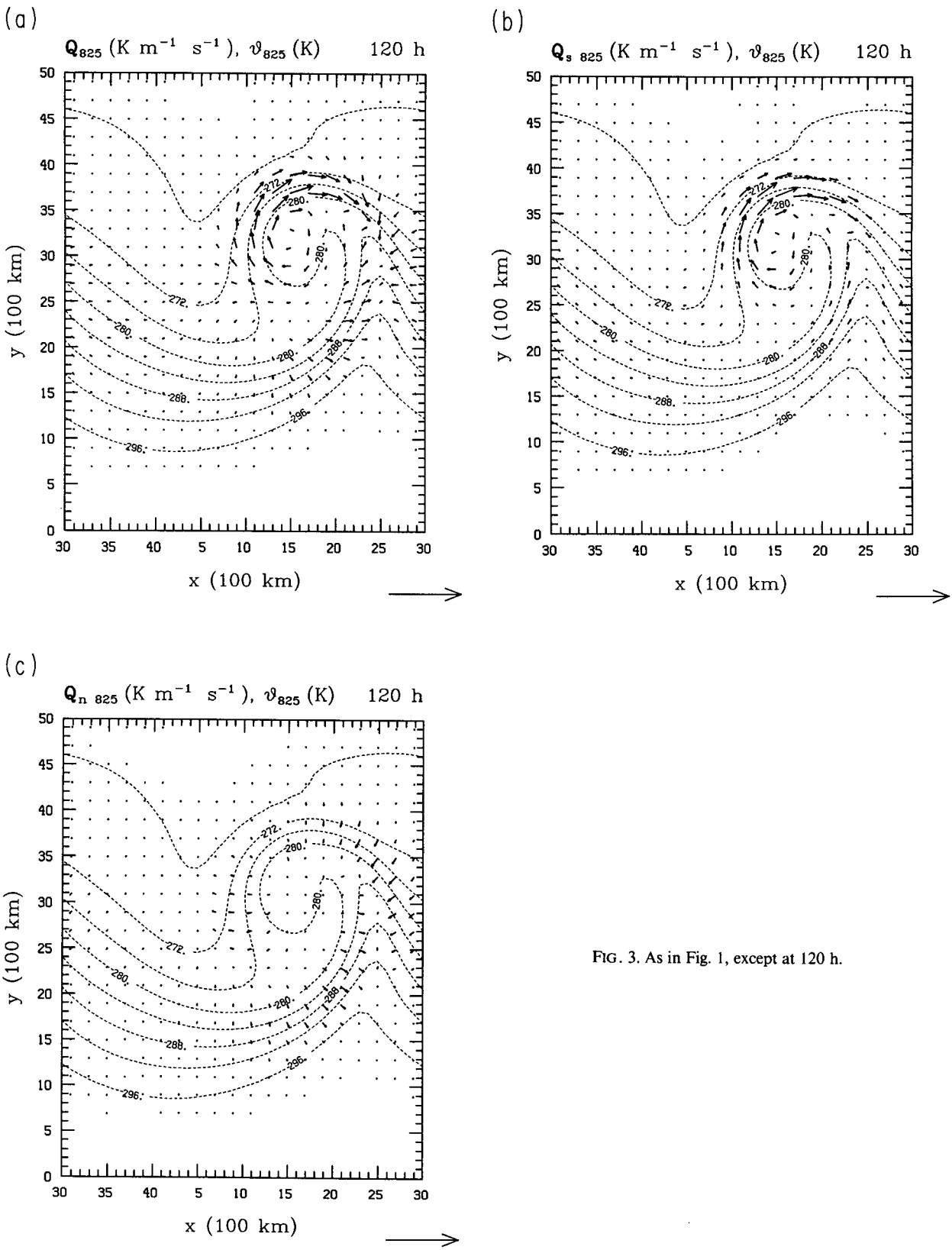

FIG. 3. As in Fig. 1, except at 120 h.

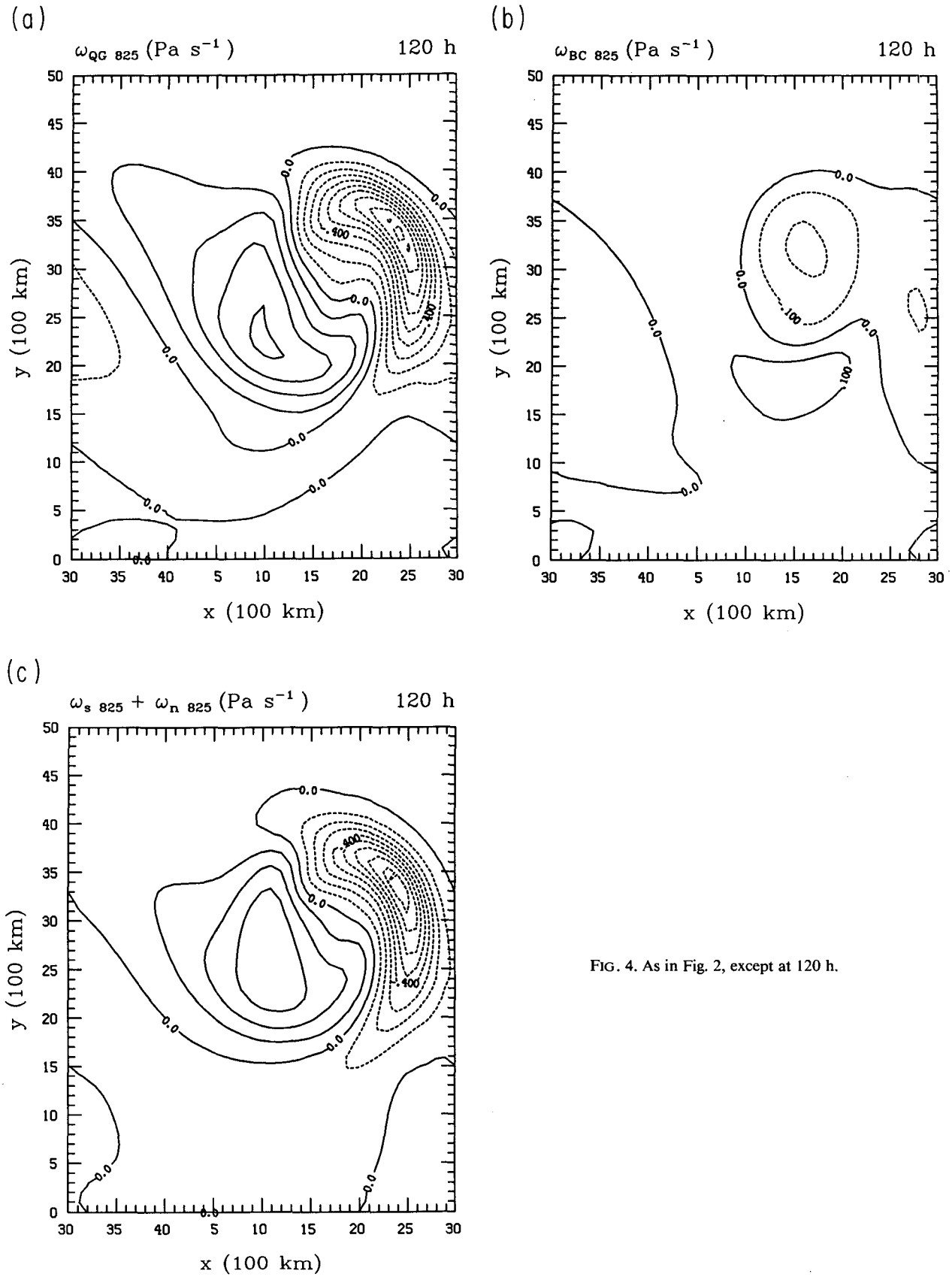

FIG. 4. As in Fig. 2, except at 120 h.

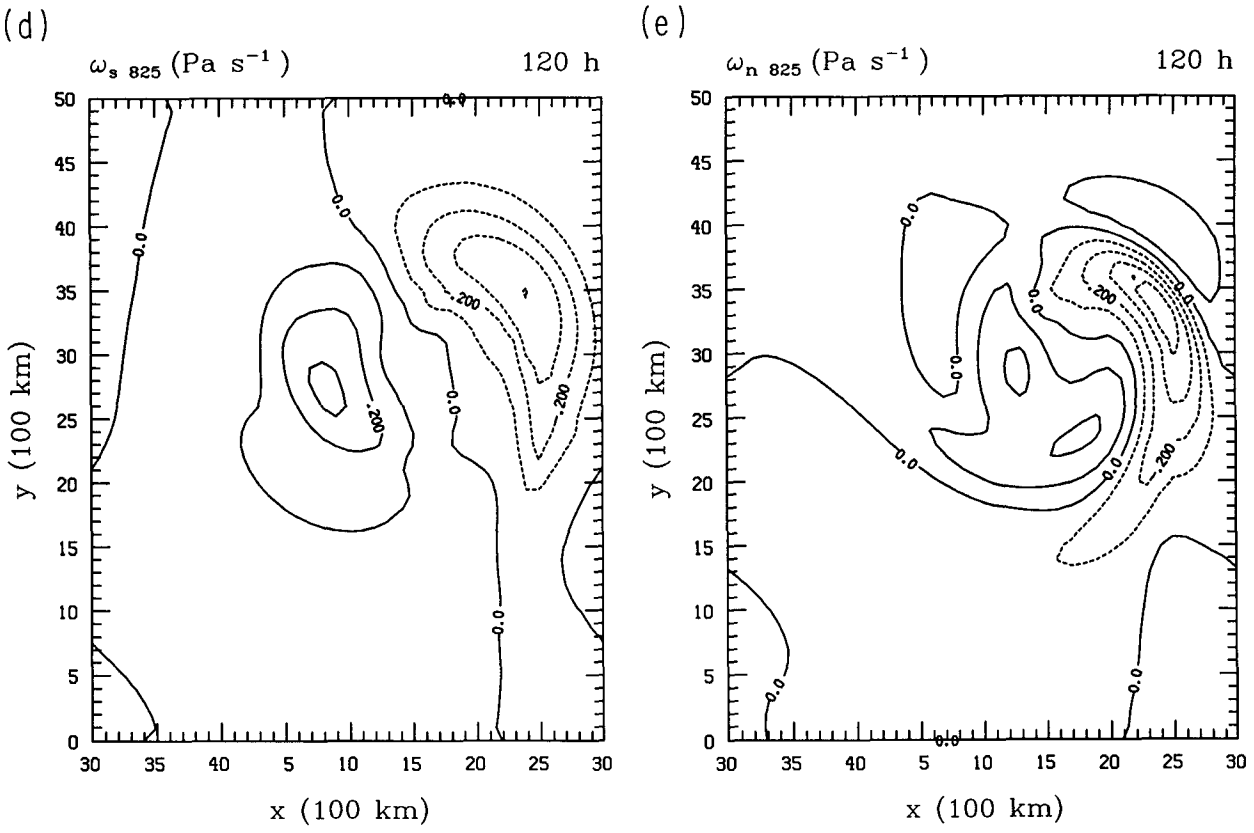

FIG. 4. (*Continued*)

of the proposed partitioning of the ω field in such a highly amplified system. A concern expressed in KRR (footnote 2) is that in large-amplitude systems the divergences of $\mathbf{Q}_s$ and $\mathbf{Q}_n$ contain contributions not only due to spatial variations of the along- and cross-isentrope components of $\mathbf{Q}$, but also due to spatial variations in the orientations of the unit vectors $\mathbf{s}$ and $\mathbf{n}$. The latter contribution may be significant when the configuration of the isentropes is highly nonlinear, that is, when the scale of the turning of the isentropes approaches that of the variation of $\mathbf{Q}_s$ and $\mathbf{Q}_n$. Another concern is that in large-amplitude systems there may be considerable vertical variations in the orientation of the thermal patterns. In such a case, the lack of coherent vertical structure potentially renders the split between $\mathbf{Q}_s$ and $\mathbf{Q}_n$ at a given level unrepresentative of a layer, thus complicating the interpretation of the resulting split between ω_s and ω_n.

The 825-hPa $\mathbf{Q}$ field (Fig. 3a) attains maximum magnitude along the *bent-back warm front,* where the orientation is primarily in the along-isentrope direction (Fig. 3b). This terminology, borrowed from the conceptual model of the low-level thermal structure of oceanic cyclones proposed by Shapiro and Keyser (1990), applies to the frontal feature that has formed poleward of the secluded region of warm air northwest of the tip of the thermal ridge in the model simulation. (Refer to Fig. 8c in KSD for a more detailed view of the low-level potential temperature structure.) As at 96 h (Fig. 1b), the configuration of $\mathbf{Q}_s$ in Fig. 3b is consistent with counterclockwise rotation of $\nabla_p\theta$ associated with westward and southwestward geostrophic flow relative to the baroclinic zone in this region (not shown). The cold- and warm-front terminology will be used to describe the baroclinic zones flanking the thermal ridge. The $\mathbf{Q}_n$ pattern (Fig. 3c) indicates frontogenesis in $|\nabla_p\theta|$ along the cold and warm fronts, the latter frontogenetical region extending into the bent-back warm front.

The total 825-hPa QG ω field (Fig. 4a) indicates the characteristic dipole pattern, the meridional extent of which has increased since 96 h (Fig. 2a), in association with the amplification of the baroclinic wave. The descent maximum is oriented along the thermal trough; the ascent maximum lies along the thermal ridge, extending along the warm side of the bent-back warm-frontal zone. The ascent pattern suggests a comma shape, as the descent region makes an indentation into the southwestern side of the ascent region, but the comma shape is not as well defined as in the PE-simulated ω field (KSD; Fig. 10a). The boundary component of ω is small (Fig. 4b), but it does contribute

somewhat to the comma shape (compare the orientations of the zero lines in Figs. 4a and 4c). The split of the ω pattern due to **Q** (Fig. 4c) into its respective components results in a dipole pattern in ω_s (Fig. 4d), with descent and ascent maxima respectively centered on the southwestern and southeastern ends of the bent-back warm front (Fig. 3b). This is similar to the distribution of the extrema in the ω_s pattern with respect to the crest of the thermal ridge at 96 h (Figs. 1b and 2d). The broadening of the zonal scales of the descent maximum toward the south, and the ascent maximum toward the north, is also apparent in the baroclinic vortex model in KRR (Fig. 10c2). The ω_n field (Fig. 4e) bears a close resemblance to its 96-h counterpart (Fig. 2e), with a relatively narrow band of ascent arcing along the bent-back warm front through the thermal ridge and then along the cold front. As at 96 h, the subsidence region is broad scale, but at this time there are maxima on the cold side of the cold-frontal zone and on the warm side of the southwestern tip of the bent-back warm front.

Although there is not a clear scale separation between the ω_s and ω_n fields at 120 h, there is evidence of a pattern separation, with ω_s contributing a cellular dipole pattern and ω_n contributing a well-defined banded feature with frontal-scale dimensions. The comma shape in the ascent pattern is seen to result from the combination of the ω_s pattern, yielding the broad "head" constituting the northern part of the ascent region, and the ω_n pattern, yielding the narrow "tail" constituting the southern part of the ascent region. The indentation in the western edge of the ascent region is formed by a combination of the ω_n and boundary-induced ω patterns.

4. Summary

The proposition in KRR that separating the **Q**-vector forcing of QG vertical motion into contributions associated with the along- and cross-isentrope components of **Q** results in a scale or pattern separation in the vertical-motion field has been considered in the case of baroclinic wave amplification and frontogenesis simulated in an f-plane PE channel model. This conjecture is based on consideration of the evolution of a passive tracer (i.e., potential temperature) in highly idealized, steady, two-dimensional flow configurations designed to isolate fundamental kinematic properties of idealized frontogenesis models and more realistic flows. Keyser et al. (1988) identified a distinct pattern separation between the forcing implied by the divergence of the along- and cross-isentrope components of **Q**, with the former yielding a dipole pattern in the forcing of descent and ascent, and the latter yielding frontal-scale bands of vertical-motion forcing. In this study, the use of a channel simulation of the evolution of a baroclinic wave disturbance to finite amplitude provides a prototype wave cyclone to test the proposition of KRR in a three-dimensional context, and the opportunity to consider the vertical motion explicitly rather than its forcing. The proposition of KRR is examined at times in the disturbance evolution when the amplitude is respectively moderate and large. In each case a pattern separation is found between the vertical-motion fields associated with the along- and cross-isentrope components of **Q**, although a distinction between the scales of the respective vertical-motion fields is not as apparent. [This discrepancy may be due in part to the relatively coarse resolution (100 km, 20 layers) of the PE model, which artificially prevents the contraction of the frontal zones to realistic limiting scales.] Overall, the along-isentrope component of **Q** yields a cellular, dipole structure, and the cross-isentrope component of **Q** yields elongated, banded structures associated with the presence of concentrated baroclinicity (frontal zones) in the flow. The distributions of vertical motion associated with the cross-isentrope component of **Q** introduce distortions to the relatively symmetric dipole pattern associated with the along-isentrope component of **Q**, resulting in asymmetries in the diagnosed vertical-motion fields reflecting the influence of frontal zones. These asymmetries thus account for the modification of the dipole pattern of descent and ascent into the comma-shaped distribution of vertical motion characteristic of midlatitude baroclinic wave disturbances.

A possible extension of this study would be to apply the proposed partitioning to observed baroclinic flow regimes.[3] One concern is the extent to which the QG-derived vertical-motion fields are appropriate reproductions of the actual vertical motions in realistic flow patterns. Use of the QG omega equation should be recognized as a limitation of this study, since comparisons of the diagnosed vertical-motion patterns with their model-simulated counterparts indicate discrepancies in amplitude and fine structure. The lack of a distinct scale separation between the vertical-motion fields forced by the along- and cross-isentrope components of **Q**, attributed above to limitations in the resolution of the PE model, may also be a consequence of the inability of the QG omega equation to reproduce details of the structure of the PE vertical motion field. Provided that the unresolved structural detail is primarily frontal scale, this characteristic of the QG omega equation may lead to the artificial broadening of the scale and reduction of the amplitude of the vertical-motion pattern associated with the cross-isentrope component of **Q**. The recently proposed "alternative balance" diagnostic model of Davies-Jones (1991) offers a promising alternative for more realistic appli-

[3] A recent example of such an application is given by M. Kurz (1990).

cations. This model retains the same form of the **Q**-vector forcing as the QG omega equation; the geostrophic wind in the expression for **Q** is replaced by the nondivergent wind, yielding the **F** vector of KRR [their Eq. (2.12)]. This diagnostic model thus should allow for greater accuracy in flow regimes where the condition of Rossby number much less than unity is violated. Provided that the alternative balance omega equation proves useful in realistic baroclinic flow regimes, additional tests may be conducted of the partitioning of the vertical-motion field investigated in this paper.

Acknowledgments. This work was initiated when the first and second authors were affiliated with the Severe Storms Branch of the Laboratory for Atmospheres, NASA/Goddard Space Flight Center and was funded by the NASA Mesoscale Atmospheric Processes Research Program. Its completion and publication was supported by the National Science Foundation through Grant ATM-8721478 and the Office of Naval Research through Contract N00014-88-K-0074. We thank Dr. Louis W. Uccellini for his administrative support of this project during the first author's transition in affiliation and the reviewers for advice in clarifying the presentation. We appreciate the assistance of Marilyn Peacock in preparing the figures.

REFERENCES

Davies-Jones, R., 1991: The frontogenetical forcing of secondary circulations. Part I: The duality and generalization of the **Q** vector. *J. Atmos. Sci.*, **48,** 497–509.

Eliassen, A., 1984: Geostrophy. *Quart. J. Roy. Meteor. Soc.*, **110,** 1–12.

Hoskins, B. J., and M. A. Pedder, 1980: The diagnosis of middle latitude synoptic development. *Quart. J. Roy. Meteor. Soc.*, **106,** 707–719.

——, I. Draghici, and H. C. Davies, 1978: A new look at the ω-equation. *Quart. J. Roy. Meteor. Soc.*, **104,** 31–38.

Keyser, D., M. J. Reeder, and R. J. Reed, 1988: A generalization of Petterssen's frontogenesis function and its relation to the forcing of vertical motion. *Mon. Wea. Rev.*, **116,** 762–780.

——, B. D. Schmidt, and D. G. Duffy, 1989: A technique for representing three-dimensional vertical circulations in baroclinic disturbances. *Mon. Wea. Rev.*, **117,** 2463–2494.

——, ——, and ——, 1992: Quasigeostrophic diagnosis of three-dimensional ageostrophic circulations in an idealized baroclinic disturbance. *Mon. Wea. Rev.*, **120,** 698–730.

Kurz, M., 1990: The forcing of vertical motions at atmospheric fronts. *Veröffentlichungen der Schweizerischen Meteorologischen Anstalt,* **48,** 205–208.

Petterssen, S., 1936: Contribution to the theory of frontogenesis. *Geofys. Publ.*, **11**(6), 1–27.

——, 1956: *Weather Analysis and Forecasting, Vol. 1. Motion and Motion Systems,* 2d ed., McGraw-Hill, 428 pp.

Sanders, F., and B. J. Hoskins, 1990: An easy method for estimation of **Q**-vectors from weather maps. *Wea. Forecasting,* **5,** 346–353.

Shapiro, M. A., and D. Keyser, 1990: Fronts, jet streams and the tropopause. *Extratropical Cyclones,* Palmén Memorial Volume, C. W. Newton and E. O. Holopainen, Eds., Amer. Meteor. Soc., 167–191.